International Journal of Multiphase Flow 36 (2010) 908–915

Contents lists available at ScienceDirect

International Journal of Multiphase Flow

journal homepage: www.elsevier.com/locate/ijmulflow

Wisp-like structures in vertical gas–liquid pipe flow revealed by wire mesh sensor studies

V. Hernandez Perez [a], B.J. Azzopardi [a,*], R. Kaji [a], M.J. da Silva [b], M. Beyer [b], U. Hampel [b]

[a] Division of Process and Environmental Engineering, Faculty of Engineering, University of Nottingham, Nottingham, NG7 2RD, UK
[b] Institute for Safety Research, Forschungszentrum Dresden-Rossendorf e.V., Dresden, Germany

ARTICLE INFO

Article history:
Received 16 January 2010
Received in revised form 3 May 2010
Accepted 4 August 2010
Available online 10 August 2010

Keywords:
Gas
Liquid vertical
Flow patterns

ABSTRACT

A conductance wire mesh sensor system has been employed on a vertical 67 mm diameter pipe with the up flow of air and water mixtures. The measuring system provides time and cross-sectionally resolved information about the spatial distribution of the phases. Statistical information can be extracted and used to identify flow patterns. The fully resolved data has revealed a hitherto unreported structure has been seen in churn flow which could be linked to the wisps in wispy-annular flow.

1. Introduction

The infinitely deformable interface between gas and liquid makes modelling of such flows difficult. Progress has been made for vertical upward flow by grouping the configurations of the interface into five flow patterns, bubbly, slug, churn, annular and wispy-annular flow, with distinctly different characteristics. They are all characterized by one or more types of periodic structures. Bubbly flow, usually described as bubbles dispersed in a liquid continuum, inevitably has a periodic variation of bubble concentration. These are termed void fraction waves by some. Slug (sometimes plug) flow consists of alternate regions of large bullet shaped bubbles which nearly fill the entire pipe cross-section and liquid regions containing clouds of small bubbles. If the pipe diameter is small enough, say ~5 mm, the liquid regions can be bubble free. The region termed churn flow is the least understood. Dukler and Hewitt have argued about its existence (Mao and Dukler, 1993; Hewitt and Jayanti, 1993; Barbosa et al., 2001). However, Sekoguchi and Mori (1997) identified that there were large periodic waves which travelled up the wall region, these they termed huge waves. In annular flow, the liquid is partitioned between drops carried by the gas travelling in the centre of the pipe and a wall film being dragged up by the gas. The film has periodic thickenings usually called disturbance waves on it. They are coherent around the circumference for small pipe diameters but Azzopardi (2006) has shown that they are more localised around parts of the periphery at larger pipe diameters. There is some evidence of periodicity in the drop concentration, though this evidence is limited (Azzopardi and Whalley, 1980; Alamu et al., 2010). Wispy-annular flow is that, high flow rate, region where annular flows are made more complex by the presence of wisps in the gas core. These are not properly understood. They appear as dark patches when viewed through a transparent pipe wall. However, that view is inevitably blurred by the wavy film interface. In examining such flows using light/detector systems mounted across pipe diameters, a periodicity distinct from the disturbance waves already present was observed (Hawkes et al., 2000). This periodicity persisted even when the liquid film (and disturbance waves) was diverted out of the pipe through a porous wall section. The occurrence of wisps has been interpreted as being the result of drop agglomeration (Hawkes et al., 2001). In contrast (Azzopardi and Wren, 2004) whilst examining the fraction of liquid removed though a porous wall section, which in annular flow is widely used to determine the fraction of liquid travelling as drops, observed that in churn flow the huge waves have a high velocity. Their high momentum flux might be sufficient to carry them past the porous wall section without being taken off. They would then be reported as entrained liquid.

The transition between bubbly and slug flow has been said to be due to the coalescence of bubbles. Taitel et al. (1980) followed the ideas of Radovcich and Moissis (1962) and suggested that coalescence would increase rapidly once the void fraction increased beyond a value of 0.25. However, Song et al. (1995) and Azzopardi (2006), amongst others have suggested that this critical void fraction depended on the ratio of mean bubble diameter to pipe diameter. Several workers, most latterly Jayanti and Hewitt (1992), have suggested that the transition between slug and churn flows is due

* Corresponding author. Tel.: +44 (0) 115 951 4160; fax: +44 115 951 4115.
E-mail address: barry.azzopardi@nottingham.ac.uk (B.J. Azzopardi).

0301-9322/$ - see front matter © 2010 Elsevier Ltd. All rights reserved.
doi:10.1016/j.ijmultiphaseflow.2010.08.002

to flooding of the falling film surrounding the Taylor bubbles. That between churn and annular flows is linked to flow reversal in the liquid film.

A complication to the above partitioning into flow patterns is that different periodic structures can occur at the same pairs of flow rates. Sekoguchi and Mori (1997) used a large number of probes mounted axially along the pipe. From the time/space data they were able to track different periodic structures and determine their velocity and height characteristics and through these apportion each structure to a specific type. The frequency of each type was then obtained. Fig. 1 shows examples of such data taken at a fixed liquid superficial velocity and illustrates how the frequencies fall and rise systematically with increasing gas superficial velocity. The frequencies of huge and disturbance waves show similarities to those of wisps and disturbance waves reported by Hawkes et al. (2000) as occurring simultaneously, Fig. 2. Further evidence of this simultaneous occurrence of periodic structures comes from Kaji et al. (2009a). They analysed the time series from four conductance ring probes mounted axially one after the other in a vertical 19 mm pipe. Specifically, they concentrated on the slug/churn boundary. By focusing on the film around Taylor bubbles in slug flow, they were able to extract the velocity of waves on the film. Many of these waves were travelling downwards. However, there were a significant majority travelling upwards. This seemed to indicate the occurrence of huge waves, typical of churn flow, in the slug flow region. The flow rates were taken near the slug/churn boundary.

This paper reports measurements taken with a wire mesh sensor system. The results are presented and discussed so as to help identify what flow patterns occur at different flow rates. The structure of the flow is also investigated.

2. Experimental arrangements

2.1. Flow facility

The experiments were carried out in an experimental facility which consists of an inclinable 6 m long rigid steel frame which can be rotated between vertical and 20° above horizontal. The test pipe of 67 mm internal diameter is mounted on the frame. In the work reported here, the pipe was mounted vertically. The fluids used were air and water. Water is taken from a storage tank and pumped into the mixer through one of a bank of flow meters to monitor the flow rate. Air from the main laboratory, 6 bar compressed-air system was monitored by one of a bank of variable area

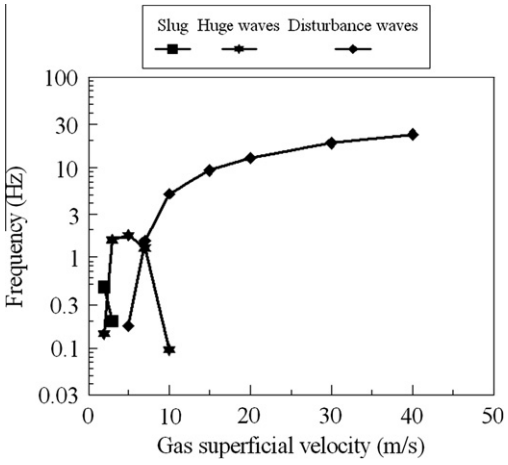

Fig. 1. Frequencies of the different periodic structures reported by Sekoguchi and Mori (1997). Pipe diameter = 26 mm, pressure = 2 bar, liquid superficial velocity = 0.1 m/s.

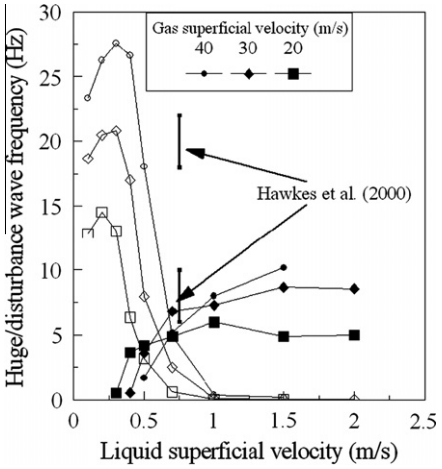

Fig. 2. Frequencies of disturbance waves, huge waves and wisps in vertical upflow. Data of Sekoguchi and Mori (1997) and Hawkes et al. (2000).

flow meters and then mixed with the water. The mixer consisted of an annular section into which the water was introduced. The air emerged into this annulus through a series of 3 mm holes on the wall of the capped central pipe. This mixer was mounted at the bottom of the test pipe and there was 5 m between this and the section where the wire mesh sensor is located. The pipe outlet is connected to a separator, the air being released to atmosphere, the water being returned to the storage tank.

2.2. Wire mesh sensor equipment

The development of an electrode mesh tomograph for high speed visualization of two-phase flows based on measurements of local instantaneous conductivity is presented in detail by Prasser et al. (1998). The operating principle of the wire mesh technique is based on a considerable difference in the electrical conductivities of the fluid pair employed. In the present experiments, the relative electrical conductivity of water is much greater than that for air. The wire mesh sensor yields a sequence of instantaneous conductivities in each crossing formed by a pair of wire electrodes (a transmitter wire, i and a receiver wire, j). For each measuring location, the instantaneous gas fraction is determined by relating the two-phase conductivity to the reference signal for the liquid phase only. This gives a three-dimensional matrix of void fractions, $\alpha_{i,j,k}$, where k is the number of measurements, i and j correspond to a pair of crossing electrode wires (transmitter and receiver).

The sensor employed in this study is shown in Fig. 3. It consists of 24 receiver and 24 transmitter wires of 250 μm diameter, which gives a measuring matrix with 24×24 elements. The distance

Fig. 3. Photograph of the 24×24 wire mesh sensor.

between the wires is 3 mm and the inner diameter of the sensor is equivalent to that of the test section. During signal acquisition, voltage pulses are supplied successively to activate the transmitter wires. The resulting currents at the receiver wires are a measure of the fluid conductivity in the control volumes surrounding the junctions of two wires. The sensor operates at frequencies of 5000 frames/s which enables small bubbles to be identified. Though most of the results reported here were taken at 1000 frames/s.

The wire mesh sensor delivers huge data volumes which require data reduction. Commonly three-dimensional image processing algorithms are used for data analysis as described by Prasser et al. (2001, 2002). This way cross-section averaged void fraction, bubble size distribution and radial profile can be extracted from the raw data. The void fraction matrix can be visualized from the measuring plane, virtual sectional side views and virtual side projections (Prasser et al., 2005). As an additional analysis method we employed Power Spectrum analysis, which gives the frequency characteristics of the flow (Kaji et al., 2009b). Here, power spectrum densities (PSD) have been obtained by using Fourier transform of auto covariance function. Since the auto covariance function has no phase lag, a discrete cosine transform can be applied.

The auto covariance function of a signal $x(t)$ is given by:

$$R_{xx}(k\Delta\tau) = \frac{1}{T-\tau}\int_0^{T-\tau}[x(t)-\overline{x}]\cdot[x(t+k\Delta\tau)-\overline{x}]dt; \quad \tau < T \qquad (1)$$

where T is the sampling duration, $k\Delta\tau$ is the time delay, τ is the interrogating time delay and

$$\overline{x} = \frac{1}{T}\int_0^T x(t)dt \qquad (2)$$

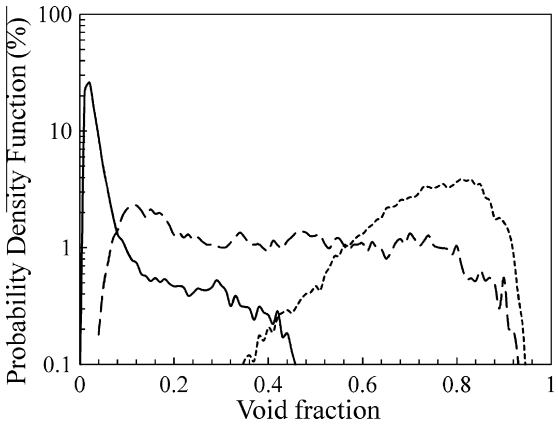

Fig. 5. Probability density functions – effect of gas superficial velocity (0.055, 0.89, 5.7 m/s; liquid superficial velocity 0.25 m/s).

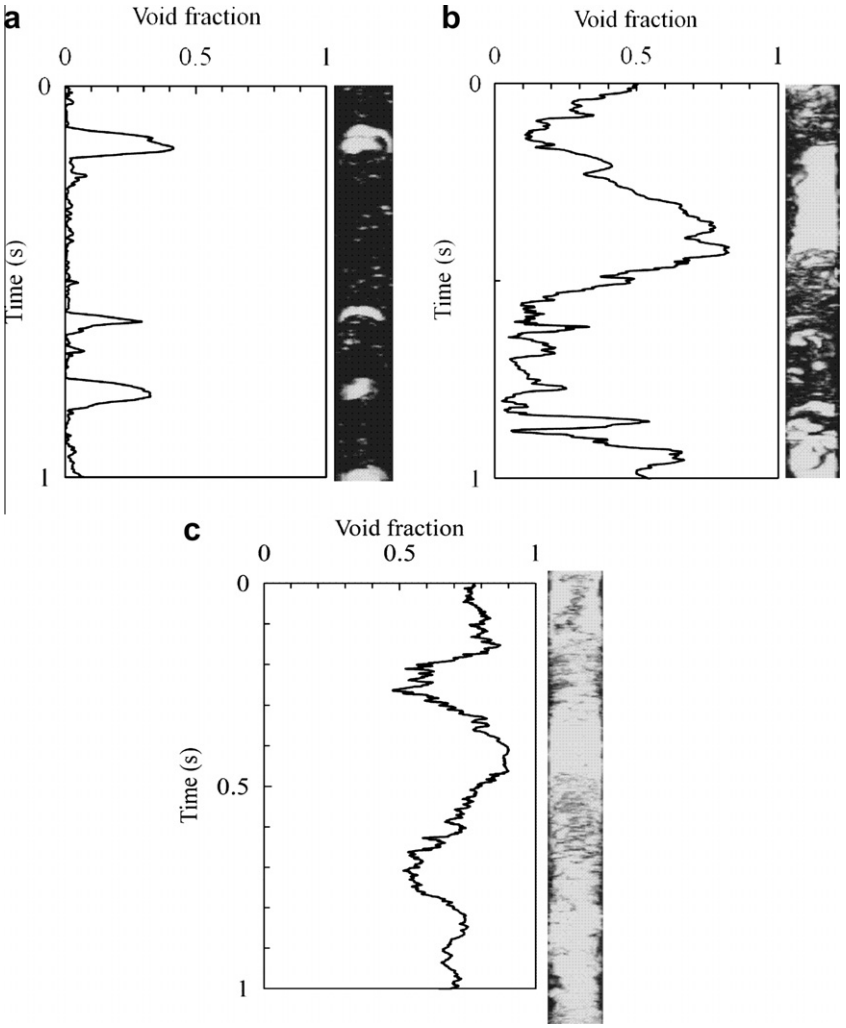

Fig. 4. Time series of cross-sectionally averaged void fraction and of void distribution across a diameter. Liquid superficial velocity = 0.25 m/s; gas superficial velocity = (a) 0.055 m/s; (b) 0.89 m/s; (c) 5.7 m/s. The case shown in (a) illustrates quite clearly a regularly spaced series of spherical cap bubbles. The one at the earliest time is a pair of bubbles coalescing. This is reflected in the double peak on the void fraction time trace.

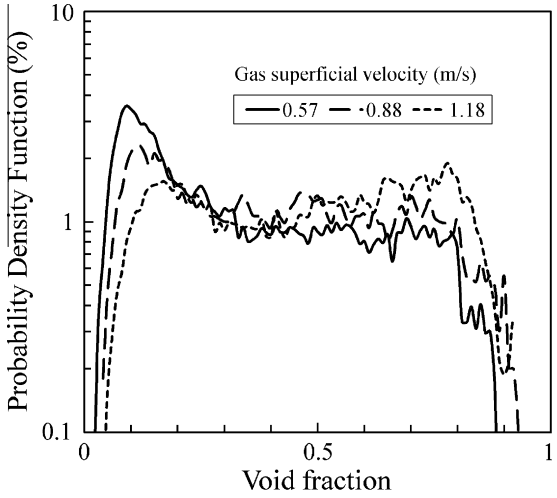

Fig. 6. Probability density functions – effect of gas superficial velocity (0.57, 0.89, 1.18 m/s; liquid superficial velocity 0.25 m/s).

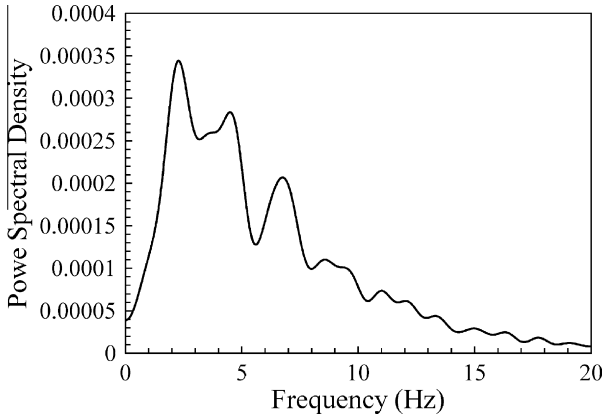

Fig. 7. Power spectral densities – gas superficial velocity = 0.055 m/s, liquid superficial velocity = 0.25 m/s.

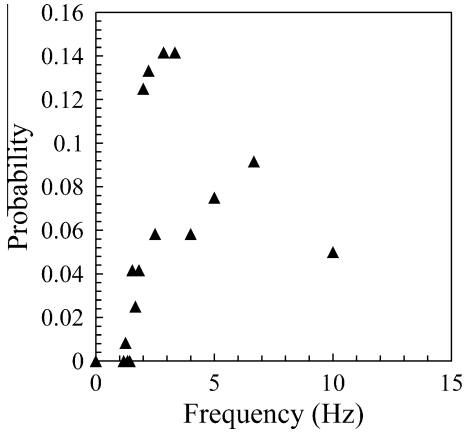

Fig. 8. Probability of occurrence of inverse of time delays between spherical cap bubbles – gas superficial velocity = 0.055 m/s, liquid superficial velocity = 0.25 m/s.

The power spectrum density is then obtained from:

$$P_{xx}(f) = \Delta\tau\left(\frac{1}{2}R_{xx}(0) + \sum_{k=1}^{\tau/\Delta\tau-1} R_{xx}(k\Delta\tau)w(k\Delta\tau)\cos(2\pi fk\Delta\tau)\right) \quad (3)$$

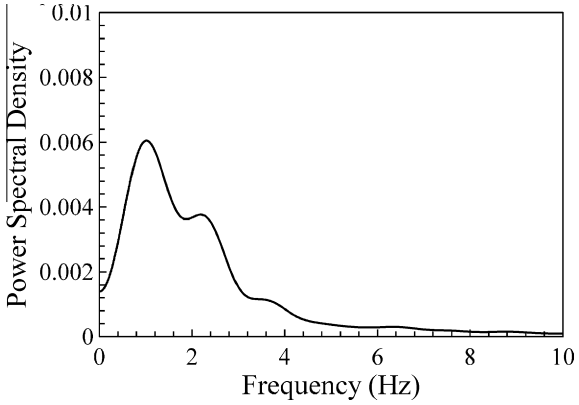

Fig. 9. Power spectral densities – gas superficial velocity = 0.89 m/s, liquid superficial velocity = 0.25 m/s.

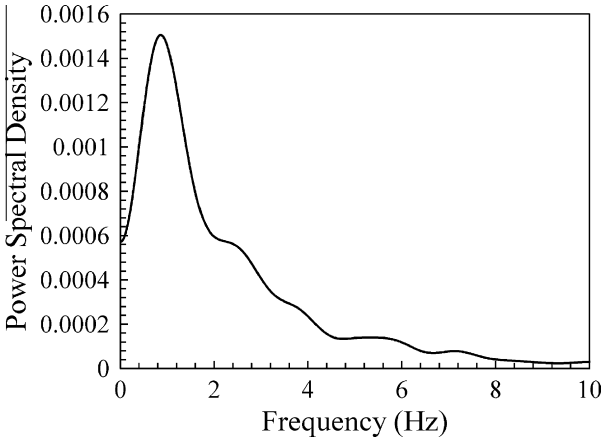

Fig. 10. Power spectral densities – gas superficial velocity = 5.7 m/s, liquid superficial velocity = 0.25 m/s.

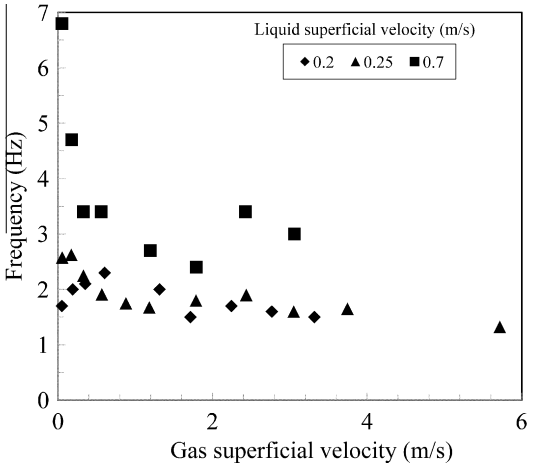

Fig. 11. Effect of gas and liquid superficial velocities on frequency.

where $w(k\Delta\tau)$ is a windowing function. Windowing functions help to suppress the spectrum leakage which mostly comes out as the sidelobes at high frequency end of the spectrum. By using appropriate windowing function the frequency contributing the system becomes clear. In the analysis carried out here, a basic cosine windowing function was used,

$$w(k\Delta\tau) = \cos\left(\frac{\pi k\Delta\tau}{2\cdot\tau}\right) \quad (4)$$

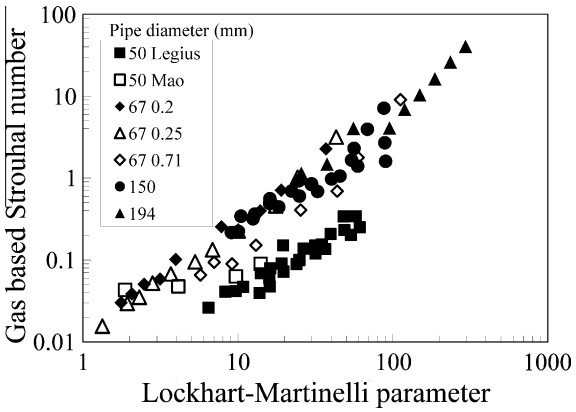

Fig. 12. Correlation of frequency – data from different pipe diameters. The second piece of information alongside the 67 mm cases is the liquid superficial velocity in m/s.

It is recognized that the wire mesh sensor intrudes into the flow. This has been subject of tests and discussion in published papers. For example, Prasser et al. (2005) comments that the shape of Taylor bubbles were significantly distorted at liquid superficial velocities up to 0.24 m/s. However, they were working at gas superficial velocities of only 0.3 m/s. At higher velocities, they found no effects.

3. Results

The flow rates at which measurements were made corresponded to gas superficial velocities in the range 0.05–5.7 m/s and liquid superficial velocities of 0.2, 0.25 and 0.7 m/s respectively. For each run data was taken at a rate of 1000 cross-sections per second for 40 s. Measurements were taken with the pipe full of water and full of air before and after each batch of tests to inform and check the calibration. A very powerful way of examining the available information is consider simultaneously the time series of cross-sectionally averaged void fraction and the times series of void fraction variation across a diameter. Examples of these are illustrated in Fig. 4. The cases were selected to be in bubbly flow (gas superficial velocity = 0.055 m/s), slug flow (0.88 m/s) and churn flow (5.7 m/s). For all the liquid superficial velocity was 0.25 m/s. The data from the lowest gas velocity is characterized by a base line of low void fraction with fairly regular peaks of higher void fraction probably representing individual spherical cap bubbles or occasionally clusters of bubbles. The intermediate gas velocity data represents the slug flow region which has alternate periods of high and low void fraction. The former come from the Taylor bubbles, the latter the liquid slugs. However, it has been observed that at these conditions there is already part of the flow that has the characteristics of churn flow. The top gas flow rate case considered here is totally in churn flow which is epitomized by a characteristic mainly high void fraction with regular troughs of lower void fraction which are probably the huge waves of Sekoguchi and Mori (1997). In each case the high and low regions can be linked directly with the more easily recognizable features in the diametric time series.

It is possible to examine this data further in two ways: through amplitude variation and time variation. The former is best carried out through the probability density function. This is the frequency of occurrence of each void fraction. The curves for the three gas superficial velocities at a liquid superficial velocity of 0.25 m/s, which were presented in Fig. 4, are shown in Fig. 5. These show the typical low void fraction peak at the lowest gas flow rate changing systematically to the highest gas flow rate where there was a peak at high void fraction with a tail to lower void fraction characteristic of churn flow. In between, there are probability density functions with a high and a low peak typical of slug flow. However, they are not as clear as those of Costigan and Whalley (1997) and Omebere-Iyari and Azzopardi (2007) who were working with

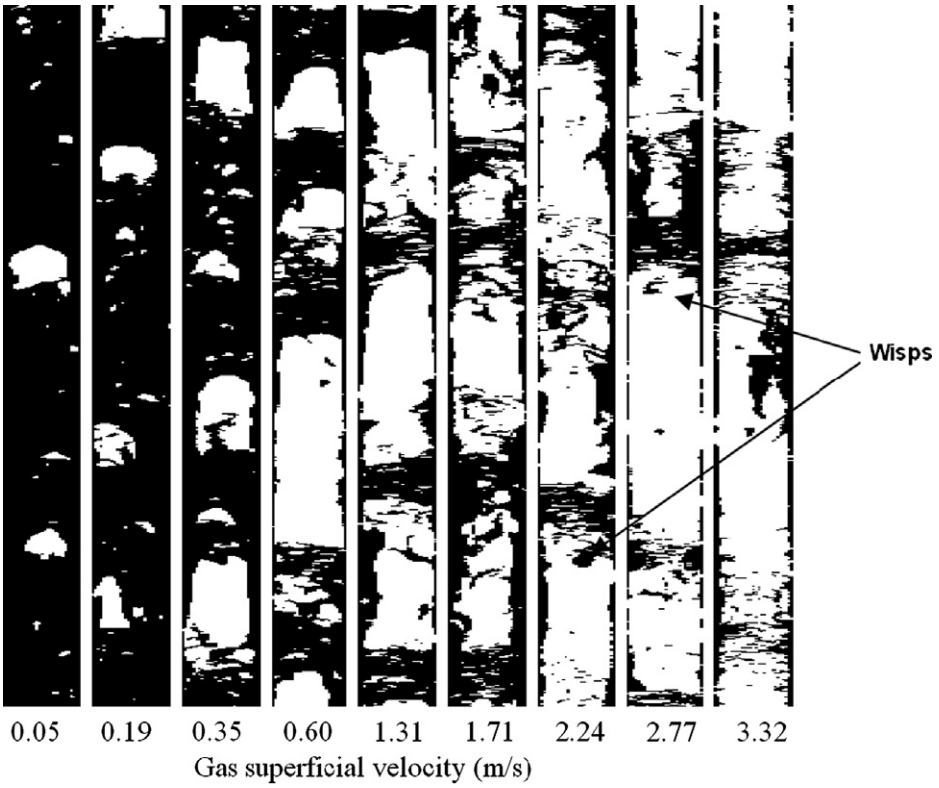

Fig. 13. Virtual side views, liquid superficial velocity = 0.2 m/s.

pipes of smaller diameter than the present experiments. The gradualness of this transition can be seen in the data presented in Fig. 6 for gas superficial velocities of 0.58, 0.88 and 1.18 m/s. Here the shift from a larger peak at low void fraction to the high void fraction peak being the higher is clearly visible.

The analysis in frequency space using power spectral density described above has been applied to the present data, particularly those considered in Fig. 4. Fig. 7 illustrates the power spectrum found for a gas superficial velocity of 0.55 m/s. This exhibits three main peaks at frequencies of 2.2, 4.4 and 6.6 Hz ($\times 1$, $\times 2$ and $\times 3$). These could be harmonics. The implications were examined further by taking the cross-sectionally averaged time trace and picking out the peaks, noting their maximum void fraction and time at which they occurred. From this the time delays between successive spherical cap bubbles were determined. From the maximum void fraction it was determined that >80% of the bubbles had a diameter >0.5 D_t where D_t is the pipe diameter. The distribution of delay times, plotted as a frequency, i.e., inverse of time delay, is shown in Fig. 8. This shows clear peaks at 2.2 and 6.6 Hz which ties in with the power spectral density. This more elaborate method of obtaining frequency has been chosen over the simple method of counting the peaks as there are doubts as which peaks should be counted.

For a gas velocity of 0.89 m/s, the power spectral density shows two peaks at frequencies of 1 and 2.2 Hz can be seen that in Fig. 9. Here it is not considered that these are harmonics but possibly the frequencies of the two types of structures seen in the time series of cross-sectionally averaged void fraction. One appears as slug flow with Taylor bubbles and liquid slugs and the other as large waves (maybe huge waves as identified by Sekoguchi and Mori, 1997). Counting the peaks in the time series plot give a frequency of about 2 Hz. Is the frequency of 1 associated with the larger structures and that of just over 2 is for the two structures combined? If the higher frequency part of the power spectral density is plotted on a log/log plot it is seen to have a slope of $-5/3$ indicating that there is a cascade of energy into high frequencies. The power spectral density of the run with a gas superficial velocity of 5.7 m/s shows only one peak – frequency = 0.8 Hz, see Fig. 10. This ties in reasonably with that obtained by counting peaks on the time trace. However, there are difficulties at deciding which peaks to include. At higher frequencies it also shows a $-5/3$ slope.

The dominant frequencies obtained from these and other runs have been extracted as above and plotted against gas superficial velocities in Fig. 11. There is no systematic trend with gas superficial velocity for values below ~0.6 m/s. Thereafter there is a general decrease with increasing gas flow rate for all liquid superficial velocities studied. There is a peak at gas superficial velocities of ~2.4 m/s whose magnitude increases with liquid superficial velocity.

The frequency of periodic structures can best be considered in terms of a dimensionless number, namely a Strouhal number (fD_t/u). Azzopardi (2004) showed that for the bubbly and slug flow region frequency data could be correlated using a gas based Strouhal number (fD/u_{gs}) and the Lockhart–Martinelli parameter, $([dp/dz]_l/[dp/dz]_g)^{0.5}$. Fig. 12 shows that data from several pipe diameters seem to lie on the same line on a log/log plot of these parameters. The data of Legius et al. (1997) from a 51 mm pipe lie on a parallel lower line. The present data from liquid superficial velocities of 0.2 and 0.25 m/s lie on the same line as those from larger pipe diameters. Those from 0.7 m/s have some data points below the bulk of the data and nearer to those of Legius. However, it is noted that for other data, Mao and Dukler (1989), taken on a pipe with the same diameter as that of Legius some agrees with Legius and some with the bulk of the data presented. It is noted that Legius et al. took their data further from the inlet mixer than the other three. Available information shows that the frequency decreases with distance from the mixer as shown by, e.g., Kaji et al. (2009c). This might explain the differences.

Examination of the virtual side views obtained from the series of cross-sectional frames gives significant insights into the flows, Fig. 13. At the lowest gas flow rate, there are individual small bubbles, usually in clusters, arriving at the wire mesh sensor. With increasing gas flow rate large bubbles, occupying most of the pipe cross-section of the pipe, occur. However, it is seen that these large bubbles do not have the very bullet shape with smooth films around them associated with the name of Taylor bubbles and which are found in small diameter pipes but have thicker, very wavy films around them. In some cases it appears that the large bubbles can be in part tight clusters of smaller bubbles. At the highest flow rates studied here there are periodic structures with high liquid contents. However, observation shows that these are not liquid continuous. There appear to be gas paths through the liquid rich areas. A more interesting feature is illustrated in Fig. 14. As well as a film on the walls, a continuous liquid object of sausage-like shape can be seen in the in the core of the Taylor bubble. Several of these objects were seen in the 40 s sequence over which data were taken. Here the interface between the film and the gas and the gas and the sausage are shown. The shape of the central liquid object is seen to be more complex at this better resolution and the curves and tendrils displayed might lead one to consider that this is an incomplete form of atomization. A very similar object was reported by Hewitt and Roberts (1969) in a 32 mm diameter pipe with gas and liquid superficial velocities of 3.5 and 2.8 m/s respectively and pressure of 4 bar. An example is shown in Fig. 15. This phenomenon can be considered as a function of the

Fig. 14. Interface between wall film and gas and gas and central liquid structure. Gas superficial velocity = 5.7 m/s; liquid superficial velocity = 0.25 m/s.

relative importance of the fluid's inertia compared to its surface tension. Therefore, a parameter that might help to relate the conditions of occurrence of the wisp in different pipes is the Weber number. The Weber number has been calculated for the conditions employed in this work ($We = \rho_g u_g^2 D/\sigma = 36$), as well as the condition at which Hewitt and Roberts (1969) observed the wisp ($We = 26$). In both cases, the Weber numbers are very similar.

4. Discussion

Wisps have been found to occur at different flow conditions. They begin to appear at gas superficial velocities as low as 1.3 m/s (Fig. 16a) in the form of large droplets (a few mm diameter) at the front of the liquid slug body, following a long Taylor bubble and their occurrence is somewhat random. When the gas superficial velocity is increased to 2.7 m/s, (Fig. 16b) they become larger and more frequent. Sometimes, for example in Fig. 16c the wisp appears to have originated from a piece of liquid falling from the front of a Taylor bubble.

In considering the sausage-like structures introduced above, it is instructive to plot the conditions at which it occurs on a flow pattern map. The transition boundaries proposed by Hewitt and Roberts (1969) are shown in Fig. 17. Also shown are the boundaries identified by Sekoguchi and Mori (1997) which are the loci of conditions where the frequency of slugs is equal to the frequency of huge waves and where the frequency of huge waves is equal to the frequency of disturbance waves. The conditions at which the structure was observed are plotted on the map. It falls between the two Sekoguchi/Mori boundaries. They also fell between the boundaries. This might be a coincidence. However, might it be that the structure is a wisp?

As expected, the wisp frequency reported in Fig. 18 increases with the gas superficial velocity, exhibiting a similar behaviour to the huge waves reported by Sekoguchi and Mori (1997), Fig. 1. However, it seems to decrease with the liquid superficial velocity, which is unexpected because the dominant structure frequency has in general been reported to increase with the liquid superficial velocity. This might be due to a high upward acceleration of liquid opposite the reversed liquid film at the back of a gas pocket, as at higher liquid superficial velocity reversed flow rarely occurs. Indeed if the liquid superficial velocity was increased even higher, wisps would be expected to disappear, giving place to the dispersed bubble flow pattern.

It might be considered that these wisp structures are an artifact of the measuring system, e.g., liquid attaching itself to the wire

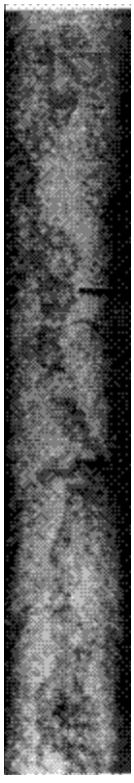

Fig. 15. Wisp recorded by X-ray photography by Hewitt and Roberts (1969). Pipe diameter 32 mm, gas superficial velocity (corrected via momentum flux to atmospheric pressure) = 7.1 m/s, liquid superficial velocity = 2.8 m/s, pressure = 4 bar.

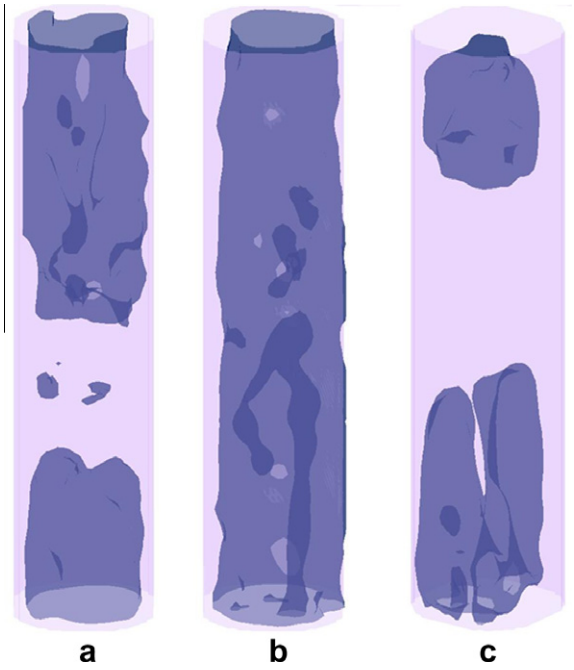

Fig. 16. Wisps found at different flow conditions. Superficial velocities (m/s) (a) liquid = 0.2, gas = 1.39; (b) liquid = 0.2, gas = 2.77; (c) liquid = 0.7, gas = 0.6.

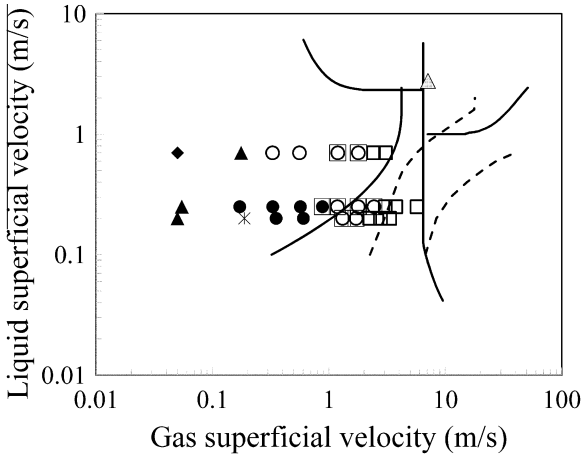

Fig. 17. Flow pattern map showing where data were taken. ■ – bubbly flow; ● – slug flow; ▲ – churn flow. Where two symbols are overlaid indicates that features of both flow patterns are present. Closed symbols indicate conditions without wisps present, open symbols are those for which wisps were observed. Also shown are the flow pattern boundaries suggested by Hewitt and Roberts (1969) and the boundaries based on equality of frequency of two simultaneously occurring periodic structures from Sekoguchi and Mori (1997). ▲ indicates the conditions at which the X-ray photograph which contained the wisps structure shown in Fig. 15 was taken.

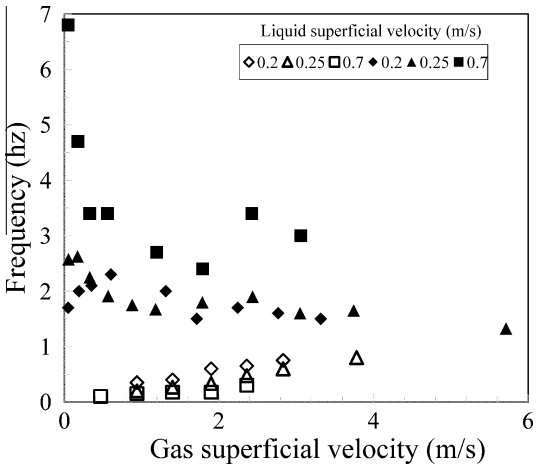

Fig. 18. Wisps frequency – open symbols – wisp frequency; closed symbols – overall frequency from power spectral density.

mesh. It is argued that they are not on two grounds. Firstly, if they were an artifact they might be expected to be less common as the gas superficial velocity increases. However, the opposite is true. Secondly, if it were a lump of liquid attached to the mesh, it might be expected that it would remain in the same position in the cross-section or oscillate about a position. The wisps identified do not do this. It might also be considered that the wisp should be visible in the time traces of cross-sectionally averaged void fraction. It would be difficult to so do as, for example the wisp illustrated in Fig. 14 would lower the void fraction by only 0.0225.

5. Conclusions

From the above the following conclusions can be drawn:

1. A new structure has been identified in the churn flow region. This takes the form of thick ligaments of liquid which have dimensions of ~10 mm diameter and be ~50 mm length.
2. The frequencies of the periodicity of the flow obtained from power spectral density analysis are seen to decrease with increasing gas superficial velocity. In contrast, the frequencies for the occurrence of wisps are seen to increase as the gas velocity is increased.

Acknowledgements

This work has been undertaken within the Joint Project on Transient Multiphase Flows and Flow Assurance. The author(s) wish to acknowledge the contributions made to this project by the UK Engineering and Physical Sciences Research Council (EPSRC) and the following: GL Industrial Services; BP Exploration; CD-adapco; Chevron; ConocoPhillips; ENI; ExxonMobil; FEESA; IFP; Institutt for Energiteknikk; PDVSA (INTEVEP); Petrobras; PETRONAS; SPT; Shell; SINTEF; Statoil and TOTAL. The authors wish to express their sincere gratitude for this support.

M.J. Da Silva acknowledges the Brazilian agency CAPES for the financial support by a doctoral grant.

References

Alamu, M.B., van der Meulen, G.P., Azzopardi, B.J., 2010, Dynamic drop size measurement in vertical annular two-phase flow. In: 7th International Conference on Multiphase Flow ICMF 2010, Tampa, FL USA, May 30–June 4.

Azzopardi, B.J., 2004. Bubbles, drops and waves: differences or underlying commonality. In: 42nd European Two-Phase Flow Group Meeting, Genoa, 23–25 June.

Azzopardi, B.J., 2006. Gas Liquid Flows. Begell House Inc., New York.

Azzopardi, B.J., Whalley, P.B., 1980. Artificial waves in annular two-phase flow. In: ASME Winter Annual Meeting, Chicago. Published in Basic Mechanisms in Two-Phase Flow and Heat-Transfer, pp. 1–8.

Azzopardi, B.J., Wren, E., 2004. What is entrainment in vertical two-phase churn flow? Int. J. Multiphase Flow 30, 89–103.

Barbosa, J., Richardson, S., Hewitt, G.F., 2001. Churn flow: myth, magic and mystery. In: 39th European Two-Phase Flow Group Meeting, Aveiro, Portugal, 18–20 June.

Costigan, G., Whalley, P.B., 1997. Slug flow regime identification from dynamic void fraction measurements in vertical air–water flows. Int. J. Multiphase Flow 23, 263–282.

Hawkes, N.J., Lawrence, C.J., Hewitt, G.F., 2000. Studies of wispy-annular flow using transient pressure gradient and optical measurements. Int. J. Multiphase Flow 26, 1562–1592.

Hawkes, N.J., Lawrence, C.J., Hewitt, G.F., 2001. Prediction of the transition from annular to wispy-annular flow using linear stability analysis of the gas-droplet core. Chem. Eng. Sci. 56, 1925–1932.

Hewitt, G.F., Roberts, D.N., 1969. Studies of two-phase patterns by simultaneous x-ray and flash photography. UKAEA Report AERE M2159.

Hewitt, G.F., Jayanti, S., 1993. To churn or not to churn. Int. J. Multiphase Flow 19, 527–529.

Jayanti, S., Hewitt, G.F., 1992. Prediction of the slug-to-churn transition in vertical two-phase flow. Int. J. Multiphase Flow 18, 847–860.

Kaji, R., Hills, J.H., Azzopardi, B.J., 2009a. Extracting information from time series data in vertical upflow. Multiphase Sci. Tech. 21, 1–12.

Kaji, R., Zhao, D., Licence, P., Azzopardi, B.J., 2009b. Studies of the interaction of ionic liquid and gas in a small-diameter bubble column. Ind. Eng. Chem. Res. 48, 7938–7944.

Kaji, R., Azzopardi, B.J., Lucas, D., 2009c. Investigation of flow development of co-current gas–liquid vertical slug flow. Int. J. Multiphase Flow 35, 335–348.

Legius, H.J.W.M., van den Akker, H.E.A., Narumo, T., 1997. Measurement of wave propagation and bubble and slug velocities in cocurrent upward two-phase flow. Exp. Therm. Fluid Sci. 15, 267–278.

Mao, Z.S., Dukler, A.E., 1989. An experimental study of gas–liquid slug flow. Exp. Fluids 8, 169–182.

Mao, Z.S., Dukler, A.E., 1993. The myth of churn flow? Int. J. Multiphase Flow 19, 377–383.

Omebere-Iyari, N.K., Azzopardi, B.J., 2007. A study of flow patterns for gas/liquid flows in small diameter tubes. Chem. Eng. Res. Des. 85, 180–192.

Prasser, H.-M., Bottger, A., Zschau, J., 1998. A new electrode-mesh tomograph for gas–liquid flows. Flow Meas. Instr., 111–119.

Prasser, H.-M., Scholz, D., Zippe, C., 2001. Bubble size measurement using wire-mesh sensors. Flow Meas. Instr. 12, 299–312.

Prasser, H.-M., Krepper, E., Lucas, D., 2002. Evolution of the two-phase flow in a vertical tube – decomposition of gas fraction profiles according to bubble size classes using wire-mesh sensors. Int. J. Therm. Sci. 41, 17–28.

Prasser, H.-M., Misawa, M., Tiseanu, I., 2005. Comparison between wire-mesh sensor and ultra-fast X-ray tomography for and air water flow in a vertical pipe. Flow Meas. Instr. 16, 73–83.

Radovcich, N.A., Moissis, R., 1962. The transition from two-phase bubble flow to slug flow. MIT Report No. 7-7673-22.

Sekoguchi, K., Mori, K., 1997. New development of experimental study on interfacial structure in gas–liquid two-phase flow. In: Giot, M., Mayinger, F., Celata, G.-P. (Eds.), Experimental Heat Transfer Fluid Mechanics and Thermodynamics, vol. 2. Edizione ETS, pp. 177–1188.

Song, C.H., No, H.C., Chung, M.K., 1995. Investigation of bubble flow developments and its transition based on the instability of void fraction waves. Int. J. Multiphase Flow 21, 381–404.

Taitel, Y., Barnea, D., Dukler, A.E., 1980. Modelling flow pattern transitions for steady upward gas–liquid flow in vertical tubes. AIChE J. 26, 345–354.